Spatial frequency tuning in human retinotopic visual areas

Linda Henriksson
Brain Research Unit of Low Temperature Laboratory and Advanced Magnetic Imaging Centre, Helsinki University of Technology, Espoo, Finland

Lauri Nurminen
Brain Research Unit of Low Temperature Laboratory and Advanced Magnetic Imaging Centre, Helsinki University of Technology, Espoo, Finland, & Department of Psychology, Faculty of Behavioural Sciences, University of Helsinki, Helsinki, Finland

Aapo Hyvärinen
Department of Computer Science, Helsinki Institute for Information Technology, University of Helsinki, Helsinki, Finland

Simo Vanni
Brain Research Unit of Low Temperature Laboratory and Advanced Magnetic Imaging Centre, Helsinki University of Technology, Espoo, Finland

Human medial occipital cortex comprises multiple visual areas, each with a distinct retinotopic representation of visual environment. We measured spatial frequency (SF) tuning curves with functional magnetic resonance imaging (fMRI) and found consistent differences between these areas. Areas V1, V2, VP, V3, V4v, and V3A were all band-pass tuned, with progressively lower SF optima in V1, V2, and V3A. In VP and V3, the SF optima were similar to optima in V2, whereas V4v showed more individual variation and scattered SF representations on the cortical surface. Area V5+ showed low-pass SF tuning. In each area, the SF optimum declined with increasing eccentricity. After accounting for the cortical magnification, the cortical extent of the optimal spatial wavelengths was approximately constant across eccentricity in V1, which suggests an anatomical constraint for the optimal SF, and this extent is actually comparable to the extent of horizontal connections within primate V1. The optimal spatial wavelengths in the visual field are also of similar extent to the spatial summation fields of macaque V1. The progressive decline in the SF tuning from V1 to V2 and V3A is compatible with the view that these areas represent visual information at different spatial scales.

Keywords: spatial frequency, eccentricity, spatial summation, spatial scale, retinotopy, fMRI

Citation: Henriksson, L., Nurminen, L., Hyvärinen, A., & Vanni, S. (2008). Spatial frequency tuning in human retinotopic visual areas. *Journal of Vision, 8*(10):5, 1–13, http://journalofvision.org/8/10/5/, doi:10.1167/8.10.5.

Introduction

Human visual cortex comprises multiple functional areas with distinct representations of the visual field. While a subset of these areas has been associated with sensitivity to specific visual features, like visual motion in area V5 (Tootell et al., 1995; Watson et al., 1993) and object shapes in area LO (Grill-Spector, Kourtzi, & Kanwisher, 2001; Malach et al., 1995), many retinotopic areas still lack characteristic functional descriptions (Wandell, Dumoulin, & Brewer, 2007). According to a model, originally based on anatomical connections, visual information is processed along a hierarchy of more sophisticated representations across early visual areas (Felleman & Van Essen, 1991; Van Essen & Gallant, 1994). This traditional view has been challenged, most recently by the finding that already neurons in the primary (V1) and the secondary (V2) visual area show complex shape selectivity (Hegdé & Van Essen, 2007).

Selectivity for spatial frequency (SF) is one of the fundamental and most thoroughly studied properties of visual neurons. For areas V1 and V2, electrophysiological and optical imaging studies on monkeys and cats suggest that alongside the retinotopic organization follows a topological representation for SF (Everson et al., 1998; Issa, Trepel, & Stryker, 2000; Xu, Anderson, & Casagrande, 2007). In monkey V1, neurons representing the same retinal location show a wide range of SF preferences, but the mean preference consistently declines as a function of visual field eccentricity (De Valois, Albrecht, & Thorell, 1982; Schiller, Finlay, & Volman, 1976; Tootell, Silverman, Hamilton, Switkes, & De Valois, 1988; Xu et al., 2007).

doi: 10.1167/8.10.5 Received February 11, 2008; published August 1, 2008 ISSN 1534-7362

At any particular eccentricity, the mean SF preference of neurons in area V2 in both cats and monkeys is on average one third as high as the preferences in area V1 (Foster, Gaska, Nagler, & Pollen, 1985; Issa et al., 2000; Movshon, Thompson, & Tolhurst, 1978). An equal ratio of the mean SF preferences has been shown between monkey areas V2 and V3 (Gegenfurtner, Kiper, & Levitt, 1997).

Previous functional magnetic resonance imaging (fMRI) studies have shown that fMRI responses in the human visual cortex are tuned for SF (Sasaki et al., 2001; Singh, Smith, & Greenlee, 2000). Singh et al. (2000) showed band-pass tuned SF response curve in V1 and low-pass tuned behavior for areas V2–V5, whereas Sasaki et al. (2001) presented for all retinotopic visual areas overall similar SF maps, in which SF preference declined with increasing eccentricity. In the present fMRI study, we explored the differences in SF tuning between human retinotopic areas at multiple eccentricities and contrast levels. Instead of Cartesian grating stimuli used in earlier studies, we used Gaussian modulated angular grating stimuli that allowed us to present a variety of SFs into the periphery without loss of eccentric specificity (Mullen, Sakurai, & Chu, 2005).

The V1 neurons are restricted to integrate visual input mainly at a local spatial scale. In macaques, the extent of this spatial summation field, measured as the area of visual field over which an expanding grating stimulus elicits an increasing response, is commensurate with the extent of V1 horizontal connections (Angelucci et al., 2002; Cavanaugh, Bair, & Movshon, 2002). We explored the possibility that some of the factors limiting the extent of these summation fields also constrain the neural population SF optima in human visual cortex.

Preliminary results of this study have been presented in the form of conference abstracts (Henriksson, Nurminen, Hyvärinen, & Vanni, 2007; Vanni, Henriksson, Nurminen, & Hyvärinen, 2007).

Methods

Overview of experiments

This study comprised four experiments. In Experiments 1 and 2, fMRI responses to grating stimuli of different spatial frequencies were measured. Both experiments covered three different visual field eccentricities and were complementary in SF range. Experiment 3 tested the effect of contrast on SF tuning. The effect of the spatial extent of the stimulus was tested in Experiment 4.

Subjects

Eight subjects participated in Experiments 1–3 and three subjects in Experiment 4 (altogether 13 different subjects, 4 females, age 23–41). All subjects had normal or corrected-to-normal vision. Ethical committee of the Hospital district of Helsinki and Uusimaa evaluated and approved the research plan, and subjects gave informed consent before participating in the study.

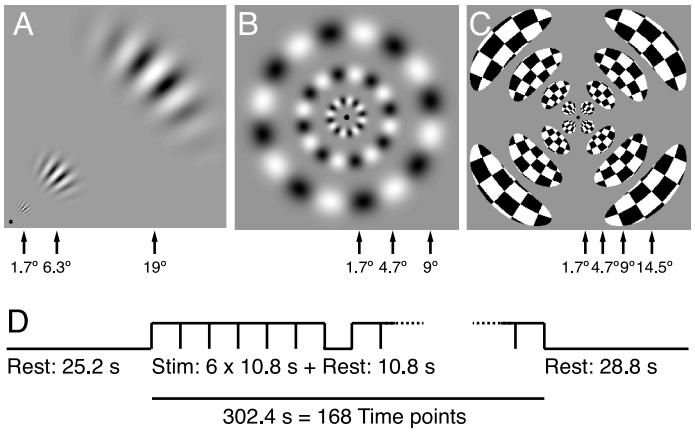

Figure 1. Spatial layouts and timing of the stimuli. (A) In Experiment 1, fMRI responses for different spatial frequencies were measured with quadrant sinring stimuli in the right upper hemifield at three eccentricities. Mean eccentricities of the stimulus patches are denoted below the stimulus frames. During an experiment, the three eccentricities were stimulated in different runs. (B) In Experiment 2, the stimulus was elongated to a ring to cover the lowest possible spatial frequencies at each eccentricity. (C) In Experiments 2 and 4, a 16-region multifocal stimulus assisted the region-of-interest selection. (D) Timing of stimuli within a run (Rest = rest period; Stim = stimulation period).

Stimuli and experimental design

The stimuli were achromatic angular sinusoidal gratings (sinrings) modulated with Gaussian envelopes both in angular (polar) and radial (eccentricity) directions (Mullen et al., 2005). Figure 1 illustrates the spatial layouts, and Table 1 illustrates the eccentricities and the spatial frequencies of the stimuli for all experiments.

Exp	Ecc (°)	SF (cyc/°)					
1	1.7	0.3	0.6	1.20	2.4	4.8	6.4
	6.3	0.15	0.3	0.6	1.2	2.4	4.8
	19	0.075	0.15	0.3	0.6	1.2	2.4
2	1.7	0.09	0.18	0.37	0.73	1.47	2.93
	4.7	0.04	0.07	0.14	0.27	0.55	1.09
	9	0.02	0.04	0.07	0.14	0.28	0.56
3–4	4.7	0.14	0.27	0.55	1.09	2.2	4.4

Table 1. Spatial frequencies (SF) and visual field eccentricities (Ecc) examined in experiments (Exp) 1–4.

In Experiment 1, the stimulation was confined to right upper visual field quadrant using Gaussian envelopes with angular space constant 15° and radial space constants for increasing eccentricities 0.3°, 0.8°, and 1.4°, which were scaled roughly to compensate for cortical magnification (Duncan & Boynton, 2003). In Experiment 2, the stimuli were elongated in the angular direction to enable the use of lowest spatial frequencies possible with an angular grating consisting of at least two cycles. In Experiments 3 and 4, a quadrant sinring stimulus at a single eccentricity was used. In Experiment 3, the contrast of this stimulus was varied, and in Experiment 4, the spatial extent of this stimulus was varied using three different angular space constants (15°, 40°, and full ring).

In all experiments, the mean luminance of the grating stimuli was 22 cd/m^2. In Experiments 1, 2, and 4, the gratings were luminance modulated with 82% maximum Michelson contrast around the mean luminance. In Experiment 3, the three different Michelson contrasts were 8.5%, 40%, and 82%. In all experiments, the gratings drifted at 4 Hz with the direction of the drift reversing every 3.6 s.

Each measurement session comprised nine functional runs. In Experiments 1 and 2, the three eccentricities were stimulated in different runs, and three runs were acquired per eccentricity. In Experiments 3 and 4, the three different conditions (Experiment 3: three contrasts; Experiment 4: three spatial layouts) alternated in separate runs, and three runs were acquired per condition. Order of spatial frequencies and conditions was pseudorandomized between the runs and the subjects. The timing of the stimuli within a run is depicted in Figure 1D. The stimuli at different spatial frequencies were presented in consecutive 10.8-s blocks. The order of these blocks was pseudorandomized and balanced across the runs. Rest periods of 10.8 s alternated the four repetitions of the stimulation periods. The first four volumes from the rest-period in the beginning of each run (7.2 s) were excluded from the analysis to reach stable magnetization.

To balance attention between conditions, subjects had to press one of the two buttons when they noticed either increase or decrease of luminance of the fixation point. The 250-ms luminance changes occurred randomly at 3–10 s. Eye movements were not recorded during the experiments, but all subjects were experienced subjects, who move their eyes on average only about 10 arcmin (Putnam et al., 2005). In Experiment 1, the grating stimulus in one visual field quadrant might attract eye movements toward the stimulus, but none of the subjects reported this. The responses for the fixation task were available for Experiment 1 for seven of the eight subjects. There were no significant differences in the correct rates or reaction times between periods of rest and stimulation, which indicates that the stimuli did not specifically interrupt fixation.

All stimuli were created with Matlab™ (Mathworks, Natick, MA), and timing was controlled with Presentation™ (Neurobehavioral Systems, Albany, CA). A 3-micromirror Christie X3™ (Christie Digital Systems, Kitchener, Ontario, CA) data projector projected the stimuli to a semitransparent screen. The subjects viewed the screen at 34 cm viewing distance via a mirror located above their eyes.

Data acquisition and analysis

Measurements were performed using a 3T GE Signa Excite scanner (General Electric Medical Systems, Milwaukee, WI) equipped with an 8-channel receiver coil. Functional volumes were acquired with echo planar imaging using single shot gradient-echo sequence. The imaging parameters were the same in each experiment. Twenty-nine slices were measured with repetition time 1.8 s, echo time 30 ms, flip angle 60°, field of view 16 cm, imaging matrix 64 × 64, and slice thickness 2.5 mm (voxel size: 2.5 mm × 2.5 mm × 2.5 mm). Structural images with low resolution (voxel size: about 1.8 mm × 1.8 mm × 1.5 mm) were acquired at the end of each session with spoiled gradient-echo sequence. These data were co-registered to high-resolution (voxel size: about 1 mm × 1 mm × 1 mm) structural images, allowing assignment of functional data onto anatomical gray-matter segmentation.

Data were analyzed with SPM2 (Wellcome Department of Imaging Neuroscience, London, UK) Matlab™ toolbox. In preprocessing, functional images were corrected for interleaved acquisition order and realigned to the functional volume measured immediately before the structural image. During the parameter estimation, the data were high-pass filtered with 140-s cut-off, and serial autocorrelations were estimated with restricted maximum likelihood algorithm using a first-order autoregressive model.

Identification of retinotopic areas

For each subject who participated in Experiments 1 and/or 2, occipital cortical surfaces were reconstructed from high-resolution anatomical images and unfolded with Brain à la Carte (BALC) Matlab™ toolbox (Warnking et al., 2002). For a subset of subjects, the initial segmentations were done with BrainVoyager QX (version 1.3, Brain Innovation, The Netherlands). Retinotopic areas V1, V2, V3/VP, V3A, and V4v were identified for each subject either with phase-encoded retinotopic mapping (Sereno et al., 1995) or with multifocal fMRI (Vanni, Henriksson, & James, 2005). The borders between retinotopic areas were delineated on the unfolded surface based on the representations of horizontal and vertical meridians. The stimulus in multifocal fMRI consisted of 24 concurrently stimulated regions in 3 rings and 8 wedges. With phase-encoded approach, the polar angle

of the visual field was mapped on the cortical surface with a rotating wedge-shaped stimulus and Fourier analysis of the response (Sereno et al., 1995; Warnking et al., 2002).

Location of visual area V5+ was identified for the individuals from the volume results without surface analysis. Identifications were based on a separate functional localizer experiment with a low-contrast (10%) concentric expanding and contracting (7°/s) stimulus. From the volume results of this experiment, the V5+ activation cluster was confirmed by checking the clusters against the known anatomical location of V5 (Watson et al., 1993). The notation V5+ indicates that this area corresponds to V5 complex, including not only V5 but also neighboring areas that are sensitive to motion.

In Experiments 3 and 4, the analysis was restricted to visual areas V1 and V2. For four subjects in Experiment 3, the occipital cortical surface reconstructions were omitted. For these subjects, the identification of visual areas V1 and V2 was based on 24-region multifocal stimulus and on checking the results of the quadrant stimulus against these multifocal responses delineating the vertical and horizontal meridian representations in the volume data.

Optimal spatial frequency maps

The topography of the SF responses was studied using optimal SF maps. These maps were created by thresholding the statistical parametric maps (threshold for volume results: $p_{FWE} < 0.05$, threshold for surface results: 1.5% signal change) and color-coding the suprathreshold voxels based on the SF corresponding to the fMRI response with the highest amplitude.

Region-of-interest analysis

The statistical parametric maps were assigned to reconstructed individual cortical surfaces for region-of-interest (ROI) analysis. To avoid biased sampling, ROIs were selected pooling together responses for all spatial frequencies and in Experiments 3 and 4 also all conditions. The locations of the maximum responses in areas V1, V2, VP, V3, V4v, and V3A in each eccentricity were marked on the individual surfaces, and corresponding voxels were selected from the statistical parametric volume maps (SPM(t)). The locations of the V5+ were marked based on the volume results for the functional localizer. Each ROI comprised voxels that exceeded threshold at $p_{FWE} < 0.05$ and were within a 4-mm radius from the marked voxel. The ROI size was limited to 3–15 voxels. ROIs were constructed separately for each experiment to exclude the effects of coregistration inaccuracies between data from different sessions.

In Experiments 2 and 4, the stimuli included full rings and correspondingly the fMRI activations spread across the visual area borders. To identify the activations in different retinotopic areas, a separate functional localizer run with a 16-region multifocal stimulus (Figure 1C; a modified stimulus from Vanni et al., 2005, four regions in each visual field quadrant, centered at 45 deg off of the meridians at eccentricities 1.7°, 4.7°, 9°, and 14.5°) was measured in the beginning of Experiments 2 and 4. Compared to the original multifocal stimulus with 60 concurrently stimulated visual field regions, the multifocal stimulus with only 16 regions activated also extrastriate areas. The multifocal activations assisted the ROI identification and construction in visual areas V1, V2, VP, and V3.

Estimates of signal changes within the ROIs were calculated from the parameter estimate images. The values of the parameter estimates within the voxels in the ROIs were divided by the corresponding mean values, multiplied by 100, and averaged (Vanni et al., 2005). The division with mean beta and multiplication by 100 reverses the global normalization of signal, implemented in SPM2 by default during parameter estimation.

Tuning curves

To visualize the SF tuning curves and to quantify the optimal SFs, Gaussian functions with logarithmic spatial frequency axis were fitted to the data

$$R = R_0 + R_1 \cdot \exp\left(-\frac{(f-\mu)^2}{2\sigma^2}\right), \quad (1)$$

where R is the fMRI response (% signal change) at a particular SF, f is the logarithm of SF, and R_0, R_1, μ and σ are parameters that were estimated using a nonlinear least squares method implemented in Matlab. These tuning curves were fitted separately for each individual data and for visualization purposes also for the SF tuning curves averaged across subjects. For each data with band-pass tuned characteristics, the fitted parameter μ indicated the optimal SF. The SF optima were averaged across subjects and visualized as a function of visual field eccentricity and visual area. To avoid biased sampling, no subject was excluded from this analysis (Figure 6), but for the individual tuning data with either low-pass or high-pass tuned characteristics, either the lowest or the highest tested SF was correspondingly defined as the optimum. The statistical significances of the differences in SF optima between visual areas, conditions, and across eccentricities were assessed with nonparametric tests; Wilcoxon signed rank test to compare two groups of paired samples and Friedman test to compare three or more groups of matched samples.

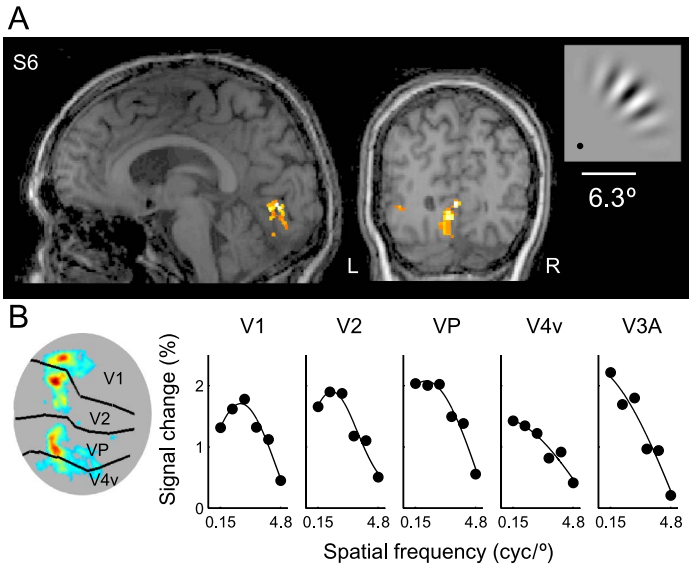

Figure 2. Single subject data from Experiment 1 for subject 6. (A) Activation pattern to 0.6 cyc/° achromatic grating stimulus at 6.3° eccentricity overlaid on individual structural MRI. (B) On the left: Activation shown in panel A assigned to subject's reconstructed and unfolded cortical surface. Borders between retinotopic visual areas were identified with phase-encoded retinotopic mapping. On the right: Signal change as a function of spatial frequency at 6.3° eccentricity shown for visual areas V1, V2, VP, V4v, and V3A.

Results

Single subject data

Experiment 1 explored the fMRI spatial frequency tuning with quadrant grating stimuli up to 19° eccentricity. Figure 2 shows representative single subject data for the middle eccentricity (6.3°) stimulus. The stimulus was confined to right upper visual field quadrant and correspondingly activated the visual areas in the left occipital cortex, more specifically the ventral division of primary visual cortex (V1), ventral division of V2, ventral posterior area (VP), areas V4v, V3A, and V5+.

The responses were quantified by fitting Gaussian functions with logarithmic spatial frequency axis to the single subject data. For this representative data (Figure 2B), the tuning curves were band-pass in visual areas V1 and V2 with peak responses at spatial frequencies 0.5 cyc/° and 0.3 cyc/°. In areas VP, V4v, and V3A, the fMRI responses increased with lower SFs, but due to limited spatial frequency range in the quadrant stimuli, an optimal SF could not be identified for these areas, i.e., the tunings appeared low-pass tuned.

In seven of the eight hemispheres, the activation topography was similar to the representative single subject data (Figure 2), and the activation foci for the sinring stimuli at different eccentricities followed the typical retinotopic organization in Experiment 1. In Experiment 2, the full rings activated both the dorsal and the ventral visual areas including areas V1, V2, VP, V3, V4v, V3A, and V5+, and the responses were sampled from representation of all four visual field quadrants. The spatial frequency range included lower SFs than tested in Experiment 1, resulting in band-pass SF tuning in all areas except V5+. The activation foci for the ring stimuli followed the typical retinotopic organization in 15 of the 16 hemispheres in Experiment 2. In one subject (S3), who participated in Experiments 1 and 2, the retinotopic organization within the left ventral occipital cortex was partially unclear both in the retinotopic data and in the sinring data.

Optimal spatial frequency maps

Figure 3 illustrates the topography of optimal spatial frequencies in the retinotopic areas for the quadrant (Experiment 1, Figures 3A and 3B) and ring (Experiment 2, Figure 3C) stimulations. Already the volume analysis (Figure 3A) reveals that the SF preference declines as a function of distance from the occipital pole, i.e., as a function of the cortical representation of visual field eccentricity. The surface analysis enables identification of retinotopic areas and confirms that in visual areas V1, V2, V3, and VP, the SF evoking the strongest response falls as a function of eccentricity (Figures 3B and 3C). The representation of low spatial frequencies is extensive in V3A. In addition, the SF maps are more fragmented on the cortical surface within areas V3A and V4v. The surface analysis shows differences in the SF optima between the visual areas. A shift in SF optima from higher to lower values follows approximately the border between areas V1 and V2 and between V3 and V3A.

Spatial frequency tuning curves in retinotopic areas

Figure 4 shows the SF tuning curves for visual areas V1, V2, VP, and V4v averaged across subjects for both quadrant (Experiment 1) and ring (Experiment 2) stimulations. Note that the signals for Experiment 2 are sampled from representation of all four visual field quadrants for visual areas V1, V2, VP, and V3 and from two visual field quadrants for areas V3A and V4v instead of one quadrant as in Experiment 1.

For visual area V1, the averaged tuning curves (Figure 4) are band-pass for all characterized eccentricities (1.7°–19°) with the peak SF declining with increasing visual field eccentricity. Due to the limited SF range that could be tested, the averaged spatial frequency tuning curves from Experiment 1 show band-pass tuning for

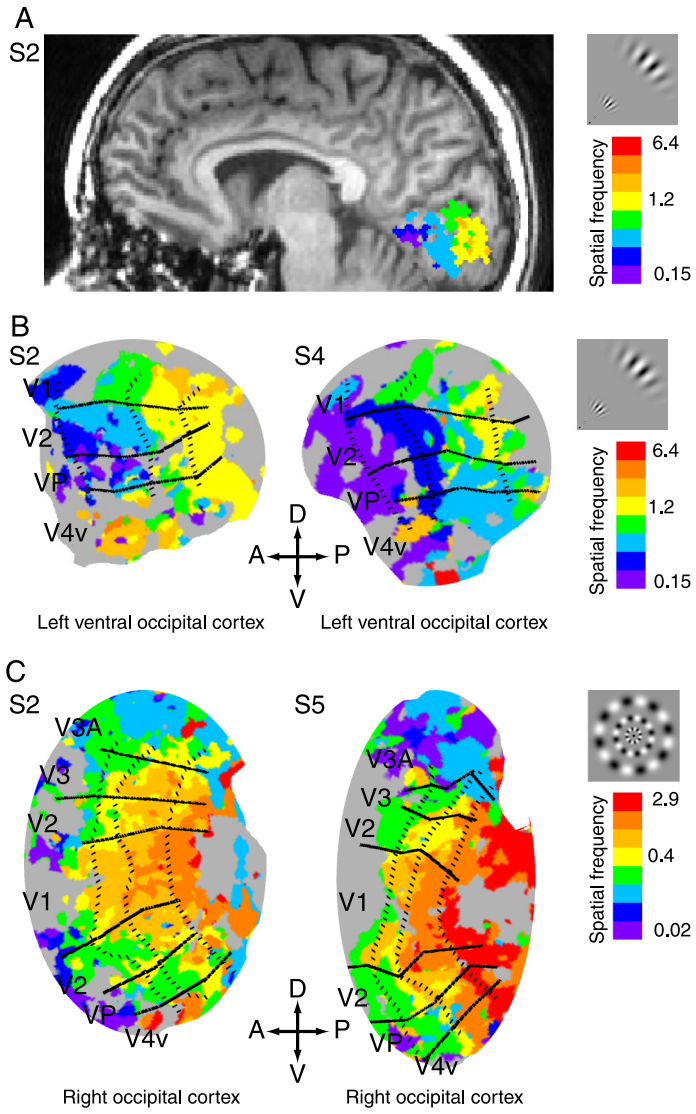

Figure 3. Optimal SF maps. (A) A map of optimal SF from Experiment 1 is shown on a left parasagittal MRI slice of Subject 2. Results from all three eccentricities are pooled together. Colors code the SF with strongest response at a particular voxel. Note that the data were not smoothed in space and only suprathreshold voxels were included, therefore resulting in somewhat sparse representations. (B) Optimal SF maps from Experiment 1 assigned to reconstructed and unfolded ventral occipital cortical surfaces of subjects S2 and S4. The solid lines indicate the borders between visual areas, and the dotted lines indicate iso-eccentricity contours. The iso-eccentricity contours were defined for the individuals based on the retinotopic mapping data and on the activation foci for the sinring stimuli at different eccentricities (D = dorsal; V = ventral; P = posterior, including the representation of fovea; A = anterior). (C) Optimal SF maps from Experiment 2 for subjects S2 and S5. Note the different SF scale.

visual areas V2, VP, and V4v only for the most foveal eccentricity. However, results from Experiment 2 with complementary SF range, show that also areas V2, VP, V3, and V4v are band-pass tuned across tested eccentricities. In addition, the peak SF in area V2 is lower compared to the peak SF in area V1. The tuning curves in areas VP and V3 appear similar to the tuning in area V2,

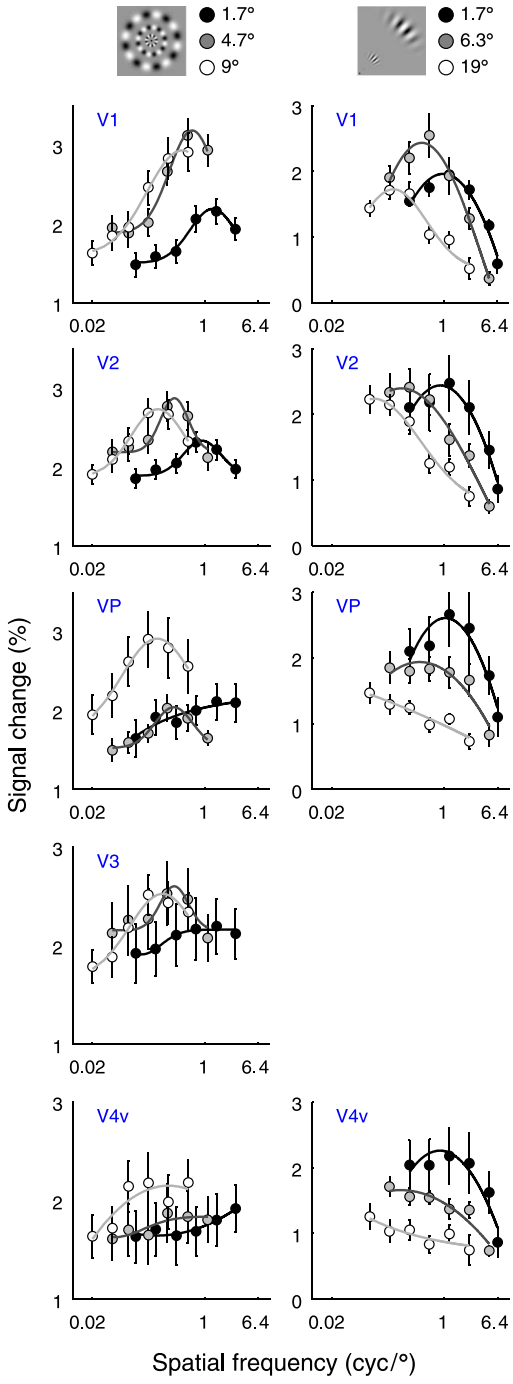

Figure 4. SF tuning curves for areas V1, V2, V3, VP, and V4v at different eccentricities averaged across subjects. The column on the left presents responses from Experiment 2 with ring stimulus and the column on the right responses from Experiment 1 with quadrant stimulus. Note the logarithmic spatial frequency axis and the different set of eccentricities and spatial frequencies in the experiments. The error bars indicate the standard errors of the means (*SEM*s).

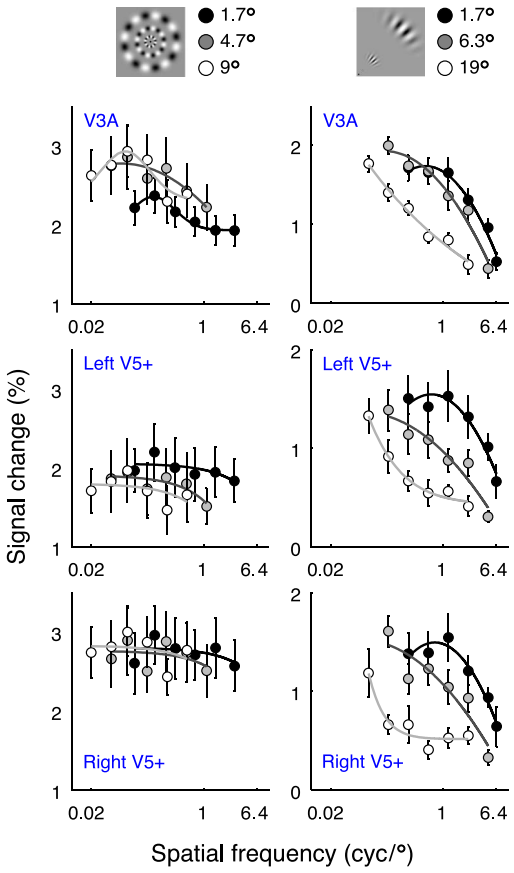

Figure 5. SF tuning curves for areas V3A and V5+ (in left and right hemispheres) at different eccentricities averaged across subjects. The column on the left presents responses from Experiment 2 with ring stimulus, and the column on the right responses from Experiment 1 with quadrant stimulus. Note the logarithmic spatial frequency axis and the different set of eccentricities and spatial frequencies in the experiments. The error bars indicate *SEM*s.

with the exception that the most foveal tuning curves appear broader than the tunings in area V2. The SF tuning in V4v differed from other data; while also band-pass tuned, the individual SF maps in V4v were more fragmented (Figure 3), and there was more variation in the tuning curves between subjects (Figure 4).

Figure 5 shows the SF tuning curves for visual areas V3A and V5+. Area V3A shows sharp high-frequency attenuation but also a modest declining in the response amplitudes at low spatial frequencies. Activation in visual motion sensitive area V5+ was evident in both hemispheres also for the quadrant stimulus. Area V5+ shows clear attenuation for high spatial frequencies but no low-frequency attenuation within the tested SF range. The cut-off frequency in the high frequency end appears, however, to shift to lower value as a function of eccentricity. The V5+ tuning curves were similar for both hemispheres.

Figure 6 shows the mean optimal spatial frequencies as a function of eccentricity for visual areas V1–V3A. Only results from Experiment 2 are shown because the SF range tested in Experiment 1 did not include low enough SFs to quantify optimal spatial frequencies across eccentricities for areas other than V1. In V1, the mean optimal spatial frequencies are 1.2 cyc/°, 0.68 cyc/°, 0.46 cyc/°, 0.40 cyc/°, and 0.18 cyc/° corresponding to eccentricities 1.7°, 4.7°, 6.3°, 9°, and 19°. Across areas V1–V3A, the visual field eccentricity had a significant effect on the optimal SF (Friedman test, $p < 0.05$). In addition, there were differences in the SF optima between areas. The SF optima were significantly higher in area V1 than in areas V2, VP, and V3A and significantly lower in area V3A than in any other area (Friedman test, $p < 0.05$). The SF optimum in area V2 was, on average, two-thirds of the SF optimum in area V1 and approximately an equal shift to a lower SF preference was observed from area V2 to area V3A. In areas VP, V3, and V4v, there was more variation in the individual tuning curves and therefore also in the mean SF optima compared to areas V1 and V2. In V4v, the mean SF optima at eccentricities 1.7° and 4.7° actually equal or exceed the SF optima in V1.

Spatial frequency tuning curves in V1 and V2 at different contrast levels

SF tuning curves shown in Figure 4 were obtained using a single contrast level (82%). Figure 7A shows the SF tuning curves at three different contrast levels averaged across subjects from Experiment 3. As shown in earlier studies (Boynton, Engel, Glover, & Heeger, 1996), the fMRI responses increased with stimulus contrast. Figure 7B illustrates the optimal spatial frequencies as a function of contrast and shows higher SF optima at lower contrast (Friedman test, $p > 0.05$). In addition, the finding of a higher SF optimum in area V1 than in V2 (Wilcoxon

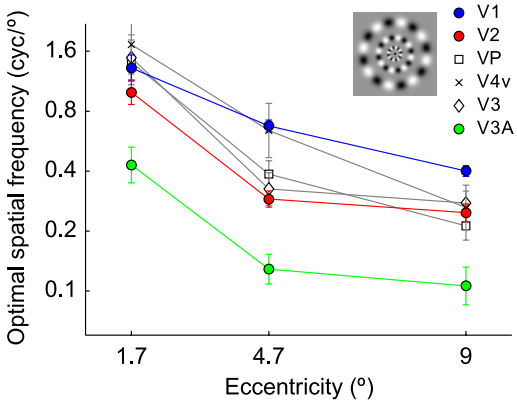

Figure 6. Optimal spatial frequencies as a function of eccentricity. The SF optima were obtained by fitting Gaussian functions of logarithmic spatial frequency to each individual tuning data and averaging across subjects the parameters indicating the optima. Error bars indicate *SEM*s. Note the logarithmic scale.

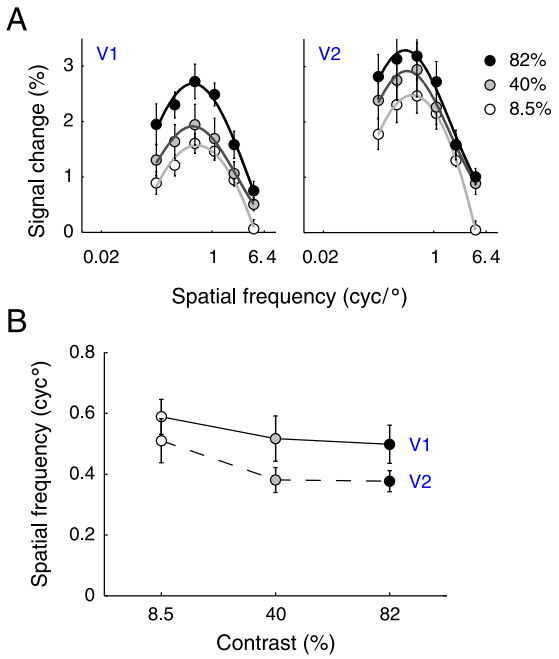

Figure 7. SF tuning curves at different contrast levels from Experiment 3 (4.7° eccentricity). (A) SF tuning curves in areas V1 and V2 at three different contrast levels averaged across subjects. (B) SF optima in areas V1 (markers connected with solid line) and V2 (markers connected with dashed line) as a function of stimulus contrast averaged across subjects. Error bars indicate *SEM*s.

signed rank test, conditions pooled together, $p < 0.01$) was repeated.

Spatial summation in V1

Experiment 4 assessed the possibility that the extent of the stimulus affects the SF tuning. Three stimulus layouts (quadrant, ring, and a layout in-between) were tested on three subjects. The results from this experiment are illustrated in Figure 8, which shows a trend of higher SF preference with larger stimulus in V2 but not in area V1. The result of a higher SF optimum in area V1 than in V2 was again repeated.

We can estimate the cortical representations for the optimal spatial wavelengths corresponding to the SF optima in V1 using an estimate of human cortical magnification (Duncan & Boynton, 2003). The representations for the optimal spatial wavelengths in V1 cortical surface are 5.3 mm, 4.0 mm, 4.7 mm, 4.0 mm, and 4.8 mm corresponding to eccentricities 1.7°, 4.7°, 6.3°, 9°, and 19°. These numbers should not be interpreted as exact measures because we did not estimate the cortical magnifications separately for each individual and because the SF optima vary between subjects. The intention here is to highlight that even though the SF preference declines as a function of eccentricity (from 1.2 cyc/° at eccentricity 1.7° to 0.18 cyc/° at eccentricity 19°) the corresponding measures of cortical distance remain approximately constant.

Discussion

This study shows that fMRI responses in human visual cortex are tuned for SF with characteristic representations in the distinct retinotopic visual areas. Areas V1, V2, VP, V3, V4v, and V3A all showed band-pass tuned responses for SF with the optimal SF declining with increasing eccentricity (Figures 4, 5, and 6). In visual area V5+, the fMRI responses showed steep attenuation for high SFs, but apparently no decrease for low SFs (Figure 5). The SF optimum in area V2 was on average two-thirds of the SF optimum in V1 and approximately an equal shift to a lower SF preference was observed from area V2 to area V3A (Figure 6). Contrast level had a modest effect on the SF tuning; at lower contrast level, the SF optima shifted to higher value (Figure 7).

Across eccentricities, the cortical representations for the optimal spatial wavelengths were approximately constant within V1, which suggests an anatomical constraint for the SF optima. We propose that the SF optima measured with fMRI reflect the size of the spatial summation field of visual neurons. Our results support the view (Hegdé & Van Essen, 2007) that human visual areas V1, V2, and V3A process visual information at progressively larger spatial scales.

Comparison with previous fMRI studies on SF processing

Sasaki et al. (2001) and Singh et al. (2000) have previously observed SF representations in the human

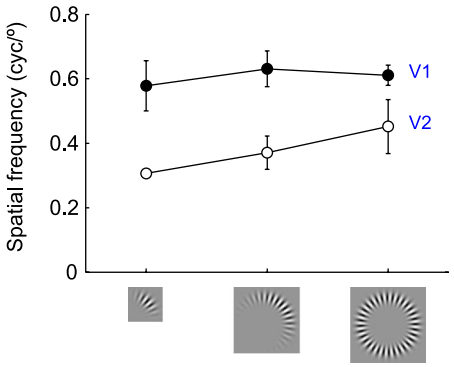

Figure 8. Optimal spatial frequencies obtained with different stimulus layouts in Experiment 4 (4.7° eccentricity). SF optima in areas V1 (black markers) and V2 (white markers) averaged across subjects are plotted as a function of stimulus layout. Angular space constants of the stimuli: 15° (quadrant), 40°, and full ring. Error bars indicate *SEM*s.

visual cortex with fMRI. The stimulus designs in these two studies and in this study differ substantially. We used sinring stimuli instead of conventional Cartesian sinusoidal gratings because sinrings allow presentation of a variety of SFs into the periphery without loss of eccentric specificity (Mullen et al., 2005). With this type of stimulus, we could complement the previous fMRI investigations with discrete measures of SF tuning curves in retinotopic visual areas. Singh et al. used a single wide-field grating (up to 15°, centered on the fovea) and reported band-pass tuning with a peak between 1 cyc/° and 4 cyc/° in area V1 and low-pass tuning in areas V2–V5. Sasaki et al. measured SF peak tuning maps with phase-encoded method and reported overall similar SF preference maps in all retinotopic areas (V1, V2, V3, VP, V3A, and V4v) with a shift in optimal SF between areas V1 and ventral V2. Our approach enabled us to report in detail differences in spatial processing between visual areas and to contribute on the discussion on the differential roles of retinotopic areas. In addition, we tested the effect of contrast level on the SF tuning.

Neural origin of fMRI spatial frequency tuning

The hemodynamic signal measured with fMRI is tightly coupled with the underlying neuronal activity (Logothetis, Pauls, Augath, Trinath, & Oeltermann, 2001). Harel, Lee, Nagaoka, Kim, and Kim (2002) showed in cats that SF tuning curves obtained using fMRI and single-cell recordings peak at similar SFs. Therefore, it seems justified to compare our fMRI results with results from single-cell studies. However, fMRI responses emerge from a population response of neural activity measured with stimulus not optimized to the preferences of single neurons. In addition, the ROIs always covered relatively large amount of cortex (3–15 voxels with dimensions 2.5 × 2.5 × 2.5 mm^3). The highest signal changes in gradient-echo fMRI might reflect voxels with contribution from draining veins. In our data, also the voxels with the maximum signal change showed clear SF tuning curves, and thus the draining veins could only have slightly relocated the activation foci.

Foster et al. (1985) reported that the mean SF preference in macaques at retinal eccentricities 2°–5° is 2.2 cyc/° in V1 and 0.65 cyc/° in V2. Similarly in cats, neurons in area 18 prefer SFs on average one third as high as those preferred in area 17 at similar retinal eccentricity (Movshon et al., 1978). Levitt, Kiper, and Movshon (1994) reported, however, substantially higher SF optima (mean 1.4 cyc/°) in macaque V2 than Foster et al. in comparable eccentricities. Our measures on humans overall agree with these results. However, the shift in the optimal SFs between areas V1 and V2 was significantly smaller than the shift reported in the single-cell studies by Foster et al. and by Movshon et al. (1978). The SF optimum in area V2 was, on average, two-thirds of the SF optimum in area V1. Our control experiment showed a trend for higher SF preference in V2 with larger stimuli. Thus, stimulus size may affect the ratio of optimal SF between areas.

In macaques, the preferred SF shifts from area V2 yet to lower values in area V3 (Gegenfurtner et al., 1997). This shift was not observed in our fMRI results, but the SF tuning in V3 appeared overall similar to the tuning in area V2. However, visual area V3A showed preference for lower SFs than V2. This is consistent with the view that human visual area V3A, rather than V3, is the most likely homologue to the macaque V3 (Singh et al., 2000; Tootell et al., 1997).

In area V4v, the optimal SF maps (Figure 3) were more fragmented and SF tuning curves wider (Figure 4) than in areas V1–V3. Signal changes were relatively high in this area, but there was more variation in the tuning curves between subjects and between neighboring voxels. With even higher signal-to-noise ratio and spatial resolution, human V4v might reveal a finer SF preference map. Single-cell recordings in the macaque monkey area V4 show a wider SF preference range and mean bandwidth compared to areas V1 and V2 (Desimone & Schein, 1987). While the human homologue to monkey V4 is not clear, the differences in our results between areas V4v and V1–V3 are commensurate with common phylogenetic history between monkey V4 and human V4v.

Spatial summation field of visual neurons

Our results on SF optima in V1 declined consistently as a function of visual field eccentricity from 1.2 cyc/° at 1.7° to 0.18 cyc/° at 19°, but the corresponding cortical representations for the optimal spatial wavelengths were approximately constant across the tested eccentricities. Similarly, the psychophysical contrast sensitivity functions measured at different eccentricities collapse to a single curve when accounted for cortical magnification (Rovamo, Virsu, & Näsänen, 1978). These results suggests that a common mechanism constraints the SF preference across eccentricity.

Our estimate of the optimal wavelength on the cortical surface (4–5 mm) is comparable to the extent of horizontal connections within primate V1 (Angelucci et al., 2002; Burkhalter & Bernardo, 1989). In macaque V1, the horizontal connections extend on average up to 6 mm in diameter with anisotropic coverage in the cortical space showing the longest connections toward fovea—a direction of summation we systematically excluded with our stimuli (Angelucci et al., 2002). A report of human local connections suggests somewhat shorter horizontal coverage with connections extending up to 4 mm in diameter (Burkhalter & Bernardo, 1989).

According to the prevailing view, the spatial summation field of a V1 neuron is covered by the local horizontal connections (Angelucci et al., 2002; Cavanaugh et al.

2002). As discussed above, our estimate of the optimal wavelength in the cortex is comparable to the extent of horizontal connections in primate V1, and in addition, our optimal spatial wavelengths in the visual field are also similar to the extents of summation fields reported in macaques at different eccentricities (Angelucci et al., 2002; Cavanaugh et al., 2002). For a single neuron in macaque or cat V1, the SF optimum and the bandwidth of the SF tuning define together the extent of receptive field (De Valois & De Valois, 1988). A neuron preferring high SF typically has a narrow spatial frequency tuning curve, and a neuron with lower SF preference has a broader SF tuning curve (Cavanaugh et al., 2002; Tolhurst & Thompson, 1981). This is also related to the number of cycles in a grating which optimally stimulates a V1 neuron. An optimal grating for a neuron preferring a high SF, i.e., a short spatial wavelength compared to the size of its summation field, comprises a relatively large number of cycles, whereas a single cycle of an optimal grating is enough to optimally stimulate a neuron with equal optimal spatial wavelength and extent of summation field (De Valois, Thorell, & Albrecht, 1985). We suggest that our neural population data on optimal spatial wavelength in human V1 reflect the extent of the horizontal connections that shape the spatial summation properties of V1 neurons and thus restrict the selective representation of low SFs. In areas V2 and V3A, the lower SF optima likely correlate with their larger summation fields.

The average receptive field (RF) sizes in human visual cortex have been estimated with fMRI using the rotating wedge-shaped and expanding ring stimuli commonly used in fMRI retinotopic mapping experiments (Dumoulin & Wandell, 2008; Smith, Singh, Williams, & Greenlee, 2001; Tootell et al., 1997). Tootell et al. (1997) introduced the idea that the progressive increase in RF size is shown up as prolonged duration of fMRI signal in response to a stimulus moving across the visual field. Smith et al. (2001) developed this technique further and reported duty cycles of these response profiles, which reflect the average RF sizes, in several retinotopic visual areas. They showed that the RF size is smallest in human V1 and increases both as a function of eccentricity and from V1 to extrastriate areas with the largest RFs in V4v and V3A. Recently, Dumoulin and Wandell (2008) introduced a quantitative population RF mapping technique and applied it to human V1, V2, V3, and lateral and ventral occipital (LO and VO) areas. In agreement with our data, the reported RFs in V2 were approximately 40% larger than the RFs in V1, but the quantitative population RF sizes in V1 were significantly smaller than our estimates for the summation fields. In electrophysiology, the classical receptive fields are typically localized by shifting a high contrast light bar across the visual field, whereas summation fields are measured as the area of visual field over which an expanding grating stimulus elicits an increasing response, which results in a response field that can be several times larger than the classical RF (Angelucci et al., 2002). It appears that the population RFs measured in fMRI with a high contrast stimulus moving across the visual field are commensurate with the electrophysiological classical receptive field measurements (Dumoulin & Wandell, 2008), whereas our measures are comparable with the summation field measurements.

Effect of contrast level on spatial frequency tuning and spatial summation

Contrast level had a modest effect on the fMRI SF tuning curves. The tuning curves in visual areas V1 and V2 peaked at slightly higher spatial frequencies at lower contrast level (Figure 7). However, single-cell measurements of macaque monkey V1 neurons show that a reduction in stimulus contrast increases spatial summation field (Sceniak, Ringach, Hawken, & Shapley, 1999) and narrows the SF bandwidth but leaves the SF preference unaffected (Sceniak, Hawken, & Shapley, 2002). Our result that SF tuning at neural population level may be differentially affected by stimulus contrast than single-cell responses is supported by findings from intrinsic optical imaging in macaque V1 and V2 (Lu & Roe, 2007). In our results and in the results by Lu and Roe (2007), the optimal SF appears to be affected by stimulus contrast, at least in area V2, and the difference in SF optima between areas V1 and V2 is more pronounced at higher contrast levels.

Relation to psychophysical CSF

The overall profile of the fMRI SF tuning in V1 agrees with the typical psychophysical contrast sensitivity function (CSF); when exceeding the optimal SF, the responses decrease steeply (Figure 4, Experiment 1), and when the SF is below the optimum, the responses decrease moderately (Figure 4, Experiment 2). In both humans and macaques, the optimal contrast sensitivity peaks around 3–5 cyc/° at fovea (De Valois, Morgan, & Snodderly, 1974). This peak shifts toward lower frequency with increasing eccentricity (Rovamo et al., 1978) and at lower light adaptation level (De Valois et al., 1974). At an adaptation level comparable to our study, the psychophysical SF optima are higher across eccentricities than our measures (Rovamo et al., 1978).

The comparison between fMRI and psychophysical data is not straightforward. Our measurements were made on high contrast stimuli unlike the contrast sensitivity measurements assessed at contrast thresholds. The difference in contrast level may be the factor shifting the physiologically measured SF optima to a lower value compared to the psychophysical optima. In our study, even the lowest contrast level (8.5%) was clearly above detection threshold, but already shifted the SF optima in

both V1 and V2 to higher values compared to a high contrast stimulus. This predicts that testing systematically contrasts down to threshold contrasts, the SF optima would increase toward the CSF results. Thorough studies with concurrent psychophysical detection tasks and fMRI measurements would provide an important link between behavioral and physiological data.

Limitations in experimental design

The drift speed of a grating is defined as the ratio of its temporal and spatial frequency. We used a single temporal frequency together with varying SFs and thus need to comprehend the relationship between SF and speed tuning. A recent study by Priebe, Lisberger, and Movshon (2006) demonstrated that simple cells in macaque V1 show separable tuning for spatial and temporal frequency and only a minority of complex cells is speed tuned. Similarly in macaque MT (the homologue for human V5), only a minority of cells shows speed-tuned behavior and the MT cells actually show a continuum from speed tuning to separable behavior (Priebe, Cassanello, & Lisberger, 2003). The speed-tuning remains a complex issue, but because the early retinotopic areas show mainly separable tuning for spatial and temporal frequency (De Valois & De Valois, 1988; Foster et al., 1985; Levitt et al., 1994; Priebe et al., 2006), our results most likely describe SF and not speed tuned characteristics.

We did not compensate our stimuli for the contrast reduction in high spatial frequencies caused by the modulation transfer function (MTF) of the projection system. We have estimated that the MTF of our projection system remains approximately constant for spatial frequencies 0.1–1 cyc/cm but is reduced approximately 15% around 2 cyc/cm (corresponding to 1.2 cyc/°) and approximately 50% around 4.5 cyc/cm (2.7 cyc/°). Thus, the reduction in contrast in the high frequency gratings in our display might have biased the SF tuning curves for the most foveal eccentricity toward lower SFs. Assuming that the extent of the cortical representation for optimal wavelength is constant across eccentricity, the real SF optima for the most foveal eccentricity is most likely near our estimate. The cortical extent of the optimal spatial wavelength in V1 was only about 0.9 mm (20%) longer for the most foveal eccentricity than the mean for other eccentricities, which suggests a reduction of only about 0.25 cyc/° in the mean SF optimum in V1.

Representations at different spatial scales

Hegdé and Van Essen (2007) reported selectivity to complex shapes already in macaque V1 and proposed that instead of a hierarchy of more sophisticated shape representations, the retinotopic areas beyond V1 analyze shapes at different spatial scales. This view is supported by Kourtzi, Tolias, Altmann, Augath, and Logothetis (2003), who showed selective fMRI activation in peripheral V1 and central V2 to collinear contours and suggested that these areas process global shapes at different spatial scales. We showed that human visual areas V1, V2, and V3A are optimally activated with stimuli of different SF content. In V1, human cortical representations of optimal spatial wavelengths corresponding to the SF optima match with the extent of human and non-human primate horizontal connections comprising the spatial summation fields. Therefore, we propose that our neural population measures of SF optima relate to the progressively larger summation fields in areas V1, V2, and V3A, and that these areas have important roles in processing visual information at progressively larger spatial scales.

Acknowledgments

We thank Marita Kattelus for help with the measurements, Antti Tarkiainen for technical support, Tarja Peromaa for discussions on display characterization, Mikko Nuutinen for the measurement of the modulation transfer function for our projection system, and Alessandra Angelucci, Pentti Laurinen, and Xtravision consortium (especially Jussi Saarinen, Jarmo Hurri, and Markku Kilpeläinen) for valuable discussions and comments on the manuscript. The Brain à la Carte toolbox was provided by unite mixte INSERM/Université Joseph Fourier 594 in Grenoble. This work was supported by Finnish Graduate School of Neuroscience, Finnish Cultural Foundation and Academy of Finland (National Programme for Centres of Excellence 2006-2011 grant 213464, grant 105628, grant 210347, and NEURO-program grant 111817).

Commercial relationships: none.
Corresponding author: Linda Henriksson.
Email: henriksson@neuro.hut.fi.
Address: Brain Research Unit, Low Temperature Laboratory, Helsinki University of Technology, P.O. Box 3000, FI-02015 TKK, Espoo, Finland.

References

Angelucci, A., Levitt, J. B., Walton, E. J., Hupe, J. M., Bullier, J., & Lund, J. S. (2002). Circuits for local and global signal integration in primary visual cortex. *Journal of Neuroscience, 22,* 8633–8646. [PubMed] [Article]

Boynton, G. M., Engel, S. A., Glover, G. H., & Heeger, D. J. (1996). Linear systems analysis of functional magnetic resonance imaging in human V1. *Journal of Neuroscience, 16,* 4207–4221. [PubMed] [Article]

Burkhalter, A., & Bernardo, K. L. (1989). Organization of corticocortical connections in human visual cortex. *Proceedings of the National Academy of Sciences of the United States of America, 86,* 1071–1075. [PubMed] [Article]

Cavanaugh, J. R., Bair, W., & Movshon, J. A. (2002). Nature and interaction of signals from the receptive field center and surround in macaque V1 neurons. *Journal of Neurophysiology, 88,* 2530–2546. [PubMed] [Article]

Desimone, R., & Schein, S. J. (1987). Visual properties of neurons in area V4 of the macaque: Sensitivity to stimulus form. *Journal of Neurophysiology, 57,* 835–868. [PubMed]

De Valois, R. L., Albrecht, D. G., & Thorell, L. G. (1982). Spatial frequency selectivity of cells in macaque visual cortex. *Vision Research, 22,* 545–559. [PubMed]

De Valois, R. L., & De Valois, K. K. (1988). *Spatial Vision*. New York: Oxford University Press.

De Valois, R. L., Morgan, H., & Snodderly, D. M. (1974). Psychophysical studies of monkey vision. 3. Spatial luminance contrast sensitivity tests of macaque and human observers. *Vision Research, 14,* 75–81. [PubMed]

De Valois, R. L., Thorell, L. G., & Albrecht, D. G. (1985). Periodicity of striate-cortex-cell receptive fields. *Journal of the Optical Society of America A, Optics and Image Science, 2,* 1115–1123. [PubMed]

Dumoulin, S. O., & Wandell, B. A. (2008). Population receptive field estimates in human visual cortex. *Neuroimage, 39,* 647–660. [PubMed]

Duncan, R. O., & Boynton, G. M. (2003). Cortical magnification within human primary visual cortex correlates with acuity thresholds. *Neuron, 38,* 659–671. [PubMed] [Article]

Everson, R. M., Prashanth, A. K., Gabbay, M., Knight, B. W., Sirovich, L., & Kaplan, E. (1998). Representation of spatial frequency and orientation in the visual cortex. *Proceedings of the National Academy of Sciences of the United States of America, 95,* 8334–8338. [PubMed] [Article]

Felleman, D. J., & Van Essen, D. C. (1991). Distributed hierarchical processing in the primate cerebral cortex. *Cerebral Cortex, 1,* 1–47. [PubMed] [Article]

Foster, K. H., Gaska, J. P., Nagler, M., & Pollen, D. A. (1985). Spatial and temporal frequency selectivity of neurones in visual cortical areas V1 and V2 of the macaque monkey. *The Journal of Physiology, 365,* 331–363. [PubMed] [Article]

Gegenfurtner, K. R., Kiper, D. C., & Levitt, J. B. (1997). Functional properties of neurons in macaque area V3. *Journal of Neurophysiology, 77,* 1906–1923. [PubMed] [Article]

Grill-Spector, K., Kourtzi, Z., & Kanwisher, N. (2001). The lateral occipital complex and its role in object recognition. *Vision Research, 41,* 1409–1422. [PubMed]

Harel, N., Lee, S. P., Nagaoka, T., Kim, D. S., & Kim, S. G. (2002). Origin of negative blood oxygenation level-dependent fMRI signals. *Journal of Cerebral Blood Flow and Metabolism, 22,* 908–917. [PubMed] [Article]

Hegdé, J., & Van Essen, D. C. (2007). A comparative study of shape representation in macaque visual areas V2 and V4. *Cerebral Cortex, 17,* 1100–1116. [PubMed]

Henriksson, L., Nurminen, L., Hyvärinen, A., & Vanni, S. (2007). *Representation of spatial frequency in human retinotopic areas* (Program No. 122.9. 2007 Neuroscience Meeting Planner). San Diego, CA: Society for Neuroscience.

Issa, N. P., Trepel, C., & Stryker, M. P. (2000). Spatial frequency maps in cat visual cortex. *Journal of Neuroscience, 20,* 8504–8514. [PubMed] [Article]

Kourtzi, Z., Tolias, A. S., Altmann, C. F., Augath, M., & Logothetis, N. K. (2003). Integration of local features into global shapes: Monkey and human FMRI studies. *Neuron, 37,* 333–346. [PubMed] [Article]

Levitt, J. B., Kiper, D. C., & Movshon, J. A. (1994). Receptive fields and functional architecture of macaque V2. *Journal of Neurophysiology, 71,* 2517–2542. [PubMed]

Logothetis, N. K., Pauls, J., Augath, M., Trinath, T., & Oeltermann, A. (2001). Neurophysiological investigation of the basis of the fMRI signal. *Nature, 412,* 150–157. [PubMed]

Lu, H. D., & Roe, A. W. (2007). Optical imaging of contrast response in macaque monkey V1 and V2. *Cerebral Cortex, 17,* 2675–2695. [PubMed] [Article]

Malach, R., Reppas, J. B., Benson, R. R., Kwong, K. K., Jiang, H., Kennedy, W. A., et al. (1995). Object-related activity revealed by functional magnetic resonance imaging in human occipital cortex. *Proceedings of the National Academy of Sciences of the United States of America, 92,* 8135–8139. [PubMed] [Article]

Movshon, J. A., Thompson, I. D., & Tolhurst, D. J. (1978). Spatial and temporal contrast sensitivity of neurones in areas 17 and 18 of the cat's visual cortex. *The Journal of Physiology, 283,* 101–120. [PubMed] [Article]

Mullen, K. T., Sakurai, M., & Chu, W. (2005). Does L/M cone opponency disappear in human periphery? *Perception, 34,* 951–959. [PubMed]

Priebe, N. J., Cassanello, C. R., & Lisberger, S. G. (2003). The neural representation of speed in macaque area MT/V5. *Journal of Neuroscience, 23,* 5650–5661. [PubMed] [Article]

Priebe, N. J., Lisberger, S. G., & Movshon, J. A. (2006). Tuning for spatiotemporal frequency and speed in directionally selective neurons of macaque striate cortex. *Journal of Neuroscience, 26,* 2941–2950. [PubMed] [Article]

Putnam, N. M., Hofer, H. J., Doble, N., Chen, L., Carroll, J., & Williams, D. R. (2005). The locus of fixation and the foveal cone mosaic. *Journal of Vision, 5*(7):3, 632–639, http://journalofvision.org/5/7/3/, doi:10.1167/5.7.3. [PubMed] [Article]

Rovamo, J., Virsu, V., & Näsänen, R. (1978). Cortical magnification factor predicts the photopic contrast sensitivity of peripheral vision. *Nature, 271,* 54–56. [PubMed]

Sasaki, Y., Hadjikhani, N., Fischl, B., Liu, A. K., Marrett, S., Dale, A. M., et al. (2001). Local and global attention are mapped retinotopically in human occipital cortex. *Proceedings of the National Academy of Sciences of the United States of America, 98,* 2077–2082. [PubMed] [Article]

Sceniak, M. P., Hawken, M. J., & Shapley, R. (2002). Contrast-dependent changes in spatial frequency tuning of macaque V1 neurons: Effects of a changing receptive field size. *Journal of Neurophysiology, 88,* 1363–1373. [PubMed] [Article]

Sceniak, M. P., Ringach, D. L., Hawken, M. J., & Shapley, R. (1999). Contrast's effect on spatial summation by macaque V1 neurons. *Nature Neuroscience, 2,* 733–739. [PubMed] [Article]

Schiller, P. H., Finlay, B. L., & Volman, S. F. (1976). Quantitative studies of single-cell properties in monkey striate cortex. III. Spatial frequency. *Journal of Neurophysiology, 39,* 1334–1351. [PubMed]

Sereno, M. I., Dale, A. M., Reppas, J. B., Kwong, K. K., Belliveau, J. W., Brady, T. J., et al. (1995). Borders of multiple visual areas in humans revealed by functional magnetic resonance imaging. *Science, 268,* 889–893. [PubMed]

Singh, K. D., Smith, A. T., & Greenlee, M. W. (2000). Spatiotemporal frequency and direction sensitivities of human visual areas measured using fMRI. *Neuroimage, 12,* 550–564. [PubMed]

Smith, A. T., Singh, K. D., Williams, A. L., & Greenlee, M. W. (2001). Estimating receptive field size from fMRI data in human striate and extrastriate visual cortex. *Cerebral Cortex, 11,* 1182–1190. [PubMed] [Article]

Tolhurst, D. J., & Thompson, I. D. (1981). On the variety of spatial frequency selectivities shown by neurons in area 17 of the cat. *Proceedings of the Royal Society of London B: Biological Sciences, 213,* 183–199. [PubMed]

Tootell, R. B., Mendola, J. D., Hadjikhani, N. K., Ledden, P. J., Liu, A. K., Reppas, J. B., et al. (1997). Functional analysis of V3A and related areas in human visual cortex. *Journal of Neuroscience, 17,* 7060–7078. [PubMed] [Article]

Tootell, R. B., Reppas, J. B., Kwong, K. K., Malach, R., Born, R. T., Brady, T. J., et al. (1995). Functional analysis of human MT and related visual cortical areas using magnetic resonance imaging. *Journal of Neuroscience, 15,* 3215–3230. [PubMed] [Article]

Tootell, R. B., Silverman, M. S., Hamilton, S. L., Switkes, E., & De Valois, R. L. (1988). Functional anatomy of macaque striate cortex: V. Spatial frequency. *Journal of Neuroscience, 8,* 1610–1624. [PubMed] [Article]

Van Essen, D. C., & Gallant, J. L. (1994). Neural mechanisms of form and motion processing in the primate visual system. *Neuron, 13,* 1–10. [PubMed]

Vanni, S., Henriksson, L., & James, A. C. (2005). Multifocal fMRI mapping of visual cortical areas. *Neuroimage, 27,* 95–105. [PubMed]

Vanni, S., Henriksson, L., Nurminen, L., & Hyvärinen, A. (2007). Topography of fMRI response for spatial frequency. *Perception, 36* (ECVP Abstract supplement).

Wandell, B. A., Dumoulin, S. O., & Brewer, A. A. (2007). Visual field maps in human cortex. *Neuron, 56,* 366–383. [PubMed]

Warnking, J., Dojat, M., Guérin-Dugué, A., Delon-Martin, C., Olympieff, S., Richard, N., et al. (2002). fMRI retinotopic mapping-step by step. *Neuroimage, 17,* 1665–1683. [PubMed]

Watson, J. D., Myers, R., Frackowiak, R. S., Hajnal, J. V., Woods, R. P., Mazziotta, J. C., et al. (1993). Area V5 of the human brain: Evidence from a combined study using positron emission tomography and magnetic resonance imaging. *Cerebral Cortex, 3,* 79–94. [PubMed]

Xu, X., Anderson, T. J., & Casagrande, V. A. (2007). How do functional maps in primary visual cortex vary with eccentricity? *Journal of Comparative Neurology, 501,* 741–755. [PubMed]